Catalyst preparation using supercritical carbon dioxide: preparation of Rh/FSM-16 catalysts and their catalytic performances in butane hydrogenolysis reaction

Paresh L. Dhepe, Atsushi Fukuoka, and Masaru Ichikawa *

Catalysis Research Center, Hokkaido University, Sapporo 060-0811, Japan

Received 31 October 2001; accepted 9 January 2002

Supported Rh catalysts on FSM-16 were prepared by treating FSM-16, impregnated with $[Rh(OAc)_2]_2$ in supercritical carbon dioxide at 398 K and 30.3 MPa, followed by calcination and hydrogen reduction. The resulting Rh/FSM-16 catalysts were characterized by CO chemisorption, XRD, TEM, FTIR and EXAFS, and catalytic performances of the Rh/FSM-16 were tested in butane hydrogenolysis reaction. It is demonstrated that highly dispersed Rh particles are obtained by the supercritical CO_2 treatment. In the hydrogenolysis reactions, the supercritical CO_2-treated catalyst showed higher conversions and ethane formation.

KEY WORDS: supercritical CO_2; catalyst preparation; supported Rh catalyst; FSM-16; butane hydrogenolysis.

1. Introduction

There is always a growing demand for highly dispersed metal particles on supports, since these supported metal catalysts are expected to show improved activity and selectivity in structure-sensitive reactions [1,2]. Generally, highly dispersed fine particles were obtained by changing the catalyst preparation procedure [2–6]. Supercritical fluids (SCFs) are attracting much attention in many fields of chemistry nowadays due to their unique properties such as high diffusivity, low viscosity, non-flammability and lack of toxicity [7–10]. SCFs are used in homogeneous, heterogeneous and biphasic catalytic reactions as a replacement to the hazardous conventional organic solvents to develop a practical process, which would be environmentally benign [7–11]. Another main advantage of SCFs is easy separation of catalyst from products after the homogeneous catalytic reactions [7,8]. SCFs were also used for the preparation of solid materials. Boyse and Ko [12] reported the use of supercritical carbon dioxide ($scCO_2$) as a drying media in the preparation of zirconia–silica aerogels. Wakayama and Fukushima [13] and Fukushima and Wakayama [14] reported the synthesis of porous silica and platinum fibers using supercritical fluid, and Poliakoff and co-workers [10,15] used the SCFs in grafting metal complexes on polymers. It has always been discussed that during the impregnation and drying process metal salts may get aggregated on supports, forming large particles that exert low dispersion. SCFs have alterable properties such as density, mass and heat transfer caused by variable temperature, pressure and other inimitable properties. We thought of taking advantage of supercritical fluids in the preparation of heterogeneous catalysts, which may help us resolve the aggregation problem. Herein preparation of FSM-16 (folded-sheet mesoporous material) [16] supported Rh catalyst is reported using $scCO_2$. Siliceous mesoporous FSM-16 has the same structure as that for MCM-41 [17] with a highly ordered hexagonal array of uniform channels. The catalysts were characterized by CO chemisorption, XRD, TEM, FTIR and EXAFS to reveal the effect of supercritical treatment on dispersion, particle-size distribution and electronic state of metal. The hydrogenolysis of lower alkanes over supported catalysts is known to be a structure-sensitive reaction, which is of great interest as a model reaction for hydrogenolysis and reforming of alkanes [1,2,18,19]. To study the differences in catalytic activity and product distribution, butane hydrogenolysis reactions were carried out over conventional Rh/FSM-16 catalyst and $scCO_2$-treated Rh/FSM-16 catalyst.

2. Experimental

$[Rh(OAc)_2]_2$ ($OAc = OCOCH_3$, Strem Chemicals, 99% pure) was used as received. FSM-16 (BET surface area 950 m^2/g, pore diameter 2.7 nm) was dried under vacuum (<0.133 Pa) at 773 K for 16 h prior to use. Tetrahydrofuran (THF) was dried over $CaC1_2$. Dry ice was used as a source of carbon dioxide, and for $scCO_2$ treatment a Hastelloy autoclave was used as a high-pressure reactor (Taiatsu TSC-002, volume 70 ml).

The procedures of catalyst preparation are shown in scheme 1. $[Rh(OAc)_2]_2$ (0.161 g, 0.364 mmol) was

* To whom correspondence should be addressed.
E-mail: michi@cat.hokudai.ac.jp

1011-372X/02/0700-0069/0

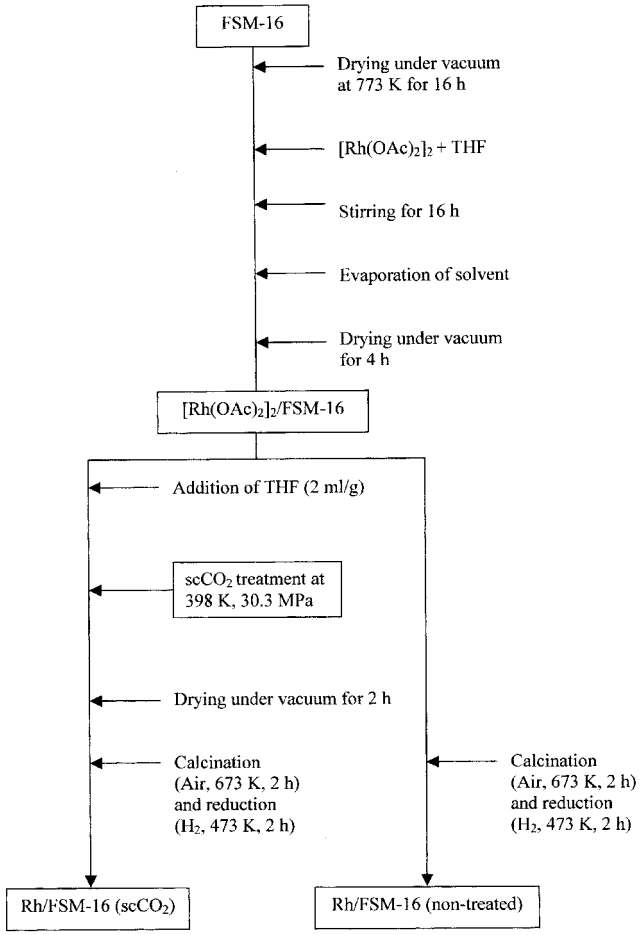

Scheme 1.

dissolved in THF (15 ml) and impregnated on 3.0 g of FSM-16 (metal loading 2.5 wt%), and the resulting mixture was stirred for 16 h. The solvent was evaporated to dryness with a rotary evaporator and then dried under vacuum (<0.133 Pa) to get a completely dry powder. This powder was then divided into two parts; one part was subjected to an $scCO_2$ treatment and the other was untreated. The $scCO_2$ treatment was given after adding a small amount of THF (2 ml/g) to the vacuum-dried powder as a co-solvent to achieve the desired properties of $scCO_2$. The $scCO_2$ treatment was performed in the autoclave at 398 K and 30.3 MPa for 24 h under stirring (CO_2: $T_c = 304$ K, $P_c = 7.4$ MPa). After releasing CO_2 the powder was dried under vacuum (<0.133 Pa). Both the non-treated and the $scCO_2$-treated catalysts were calcined in air at 673 K for 2 h and reduced under a flow of H_2 (20 ml/min) at 473 K for 2 h. Hereafter, we will use abbreviations: Rh/FSM-16 ($scCO_2$) for the $scCO_2$-treated Rh/FSM-16 catalyst and Rh/FSM-16 (non-treated) for the conventional Rh/FSM-16, non-treated catalyst.

CO uptake was carried out for measurement of dispersion and particle size on an Altamira AMI1 instrument in a pulse-adsorption mode with a thermal conductivity detector (TCD). Chemisorption was measured at 323 K to ensure no contribution from physically adsorbed CO molecules on the support surface. Powder X-ray diffraction (XRD) was done on a Rigaku MiniFlex using Cu K_α radiation. Transmission electron microscopy (TEM) was performed on a Hitachi H-800 instrument at 200 kV. IR spectra were recorded at 298 K using a Shimadzu FTIR 8100 M with a resolution of 2 cm^{-1}. Co-accumulation of 100 interferograms was done to improve the signal/noise ratios of IR spectra. For IR analysis, powder samples (15–20 mg) were pressed into a self-supporting wafer (diameter 1.9 cm) with a pressure of 49 MPa. The wafer was mounted in an *in situ* IR cell equipped with CaF_2 windows. Before adsorption of CO, the sample wafer was reduced at 473 K for 1 h under H_2 atmosphere (26.6 kPa). After reduction the cell was evacuated at 473 K for 30 min and cooled to room temperature. For the IR spectroscopy of CO adsorption, CO (26.6 kPa) was adsorbed on the sample wafer at 298 K for 1 h. Then the IR cell was evacuated for 2 min. XAFS spectra were measured at 296 K at BL-10B of the Photon Factory of High Energy Accelerator Research Organization (KEK-PF, Tsukuba), and the XAFS data were analyzed by a REX 2000 program (Rigaku).

The hydrogenolysis of butane was performed in a flow system with a quartz tube reactor. Rh/FSM-16 catalyst (0.15 g, Rh 2.5 wt%, 20–42 mesh) was charged in the reactor and was reduced in H_2 flow (20 ml/min) at 523 K for 30 min to clean the surface of the catalyst. After the H_2 reduction, the catalyst was cooled to the desired reaction temperature in flowing H_2. Then a gas mixture of H_2 and n-C_4H_{10} was introduced into the catalyst bed under the following conditions: 101 kPa, H_2:n-$C_4H_{10} = 9:1$, GHSV = 3800 h^{-1}. Gaseous products were analyzed by gas chromatograph (Shimadzu GC-8A) equipped with a 3 m Unibeads A column and a TCD. The concentrations of the products were first calibrated with a standard gas mixture. In order to ensure the steady state of the reaction achieved, off-gas was analyzed on GC after each hour of the reaction time. Results presented here are after 4 h of total reaction time at which steady state was observed.

3. Results and discussion

3.1. Preparation and characterization of catalysts

Much study of $scCO_2$ treatments gave us the idea that the addition of a little amount of co-solvent was necessary for better dispersion of Rh on FSM-16 support. Accordingly, a small amount of THF was used as a co-solvent before the $scCO_2$ treatment as described in section 2 and scheme 1. Different metal precursors were used in the catalyst preparation such as $RhCl_3 \cdot 3H_2O$, $Rh(acac)_3$ and $Rh_4(CO)_{12}$. Among these precursors, $RhCl_3 \cdot 3H_2O$ and $Rh_4(CO)_{12}$ were decomposed under our $scCO_2$-treatment conditions forming black metal particles on the support. $Rh(acac)_3$ was volatile and was observed on

Table 1
Results of CO chemisorption [a]

Catalyst	CO/Rh	Mean particle diameter (nm) [b]
Rh/FSM-16 ($scCO_2$)	0.71	1.5
Rh/FSM-16 (non-treated)	0.15	7.4

[a] CO (101 kPa) in the pulse mode.
[b] According to the spherical model in ref. [20].

the inner walls of the reactor after treatment. After many trials, $[Rh(OAc)_2]_2$ was found to be the most suitable precursor for preparation of Rh/FSM-16 catalyst with $scCO_2$. It has solubility in THF and is miscible with $scCO_2$. Its green color was retained after the $scCO_2$ treatment, indicating no decomposition of the complex.

Results obtained from the volumetric CO chemisorption after calcination and reduction are presented in table 1. As the data show, the Rh/FSM-16 ($scCO_2$) catalyst has a higher metal dispersion of 71% compared with the Rh/FSM-16 (non-treated) catalyst (15%). From the dispersion data, the mean particle size was calculated to be 1.5 and 7.4 nm respectively, assuming a spherical rhodium particle model [20]. This indicates that after the $scCO_2$ treatment fine Rh particles were formed on the FSM-16 support.

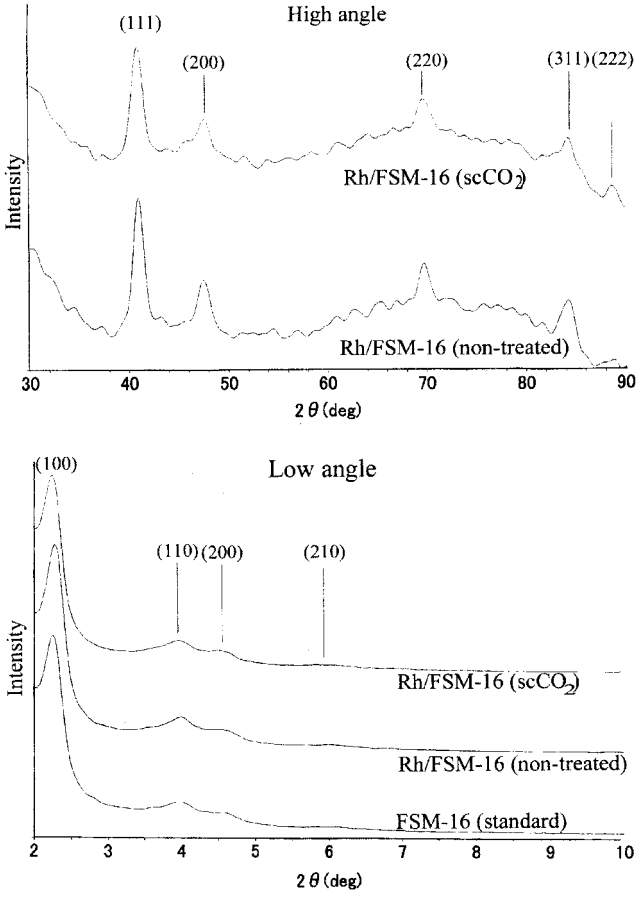

Figure 1. XRD patterns of Rh/FSM-16 catalysts: (a) high-angle region and (b) low-angle region.

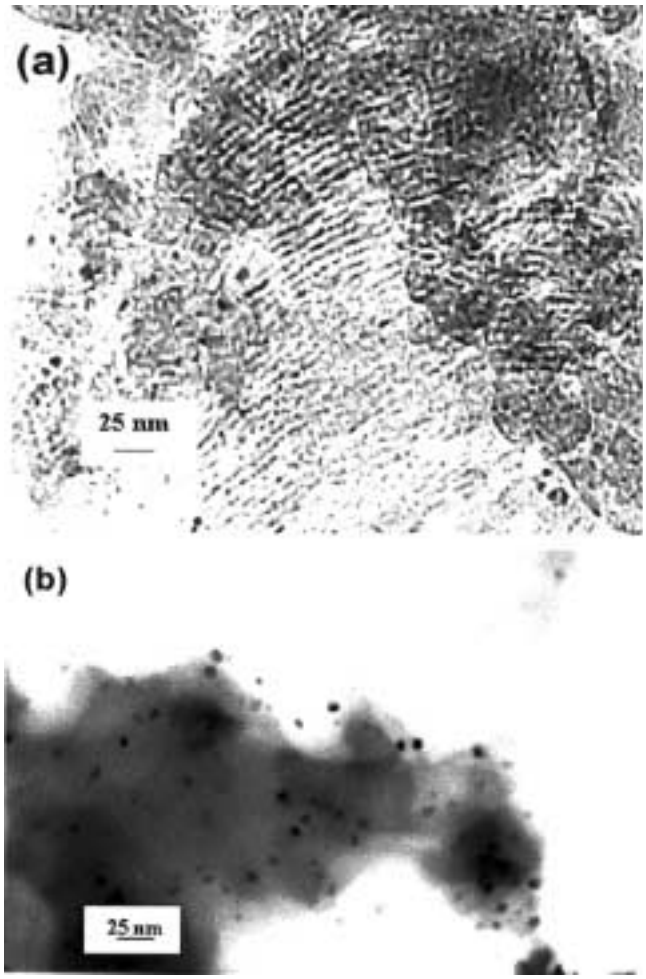

Figure 2. TEM images of Rh/FSM-16 catalysts: (a) Rh/FSM-16 ($scCO_2$) and (b) Rh/FSM-16 (non-treated).

XRD patterns for the catalysts are shown in figure 1. For the Rh/FSM-16 ($scCO_2$), the same diffraction patterns due to a 2D hexagonal structure were observed in the low-angle region (2–10°) as that for the standard FSM-16. This shows that the pore structure of FSM-16 is preserved in the $scCO_2$ treatment. In the high-angle region at 30–90°, typical diffraction patterns of fcc Rh crystalline were obtained.

TEM was employed to study the microstructure of FSM-16, the location and size of the metal particles. In figure 2(a), Rh particles are observed as dark spots with a mean particle size of 2.0 nm, which implies that the Rh particles are situated inside the channels. For the Rh/FSM-16 (non-treated) catalyst in figure 2(b), big Rh particles are seen and their mean diameter is 4.0 nm, indicating the formation of Rh particles on the external surface of FSM-16.

XAFS studies were performed for the structural characterization of catalysts. Figure 3(a) shows Fourier transforms of k^3-weighted EXAFS functions $\chi(k)$ for the Rh/FSM-16 catalysts and Rh foil. The major peaks are observed at 0.23 nm without phase shift correlation due to the first Rh–Rh shell, and their peak intensities

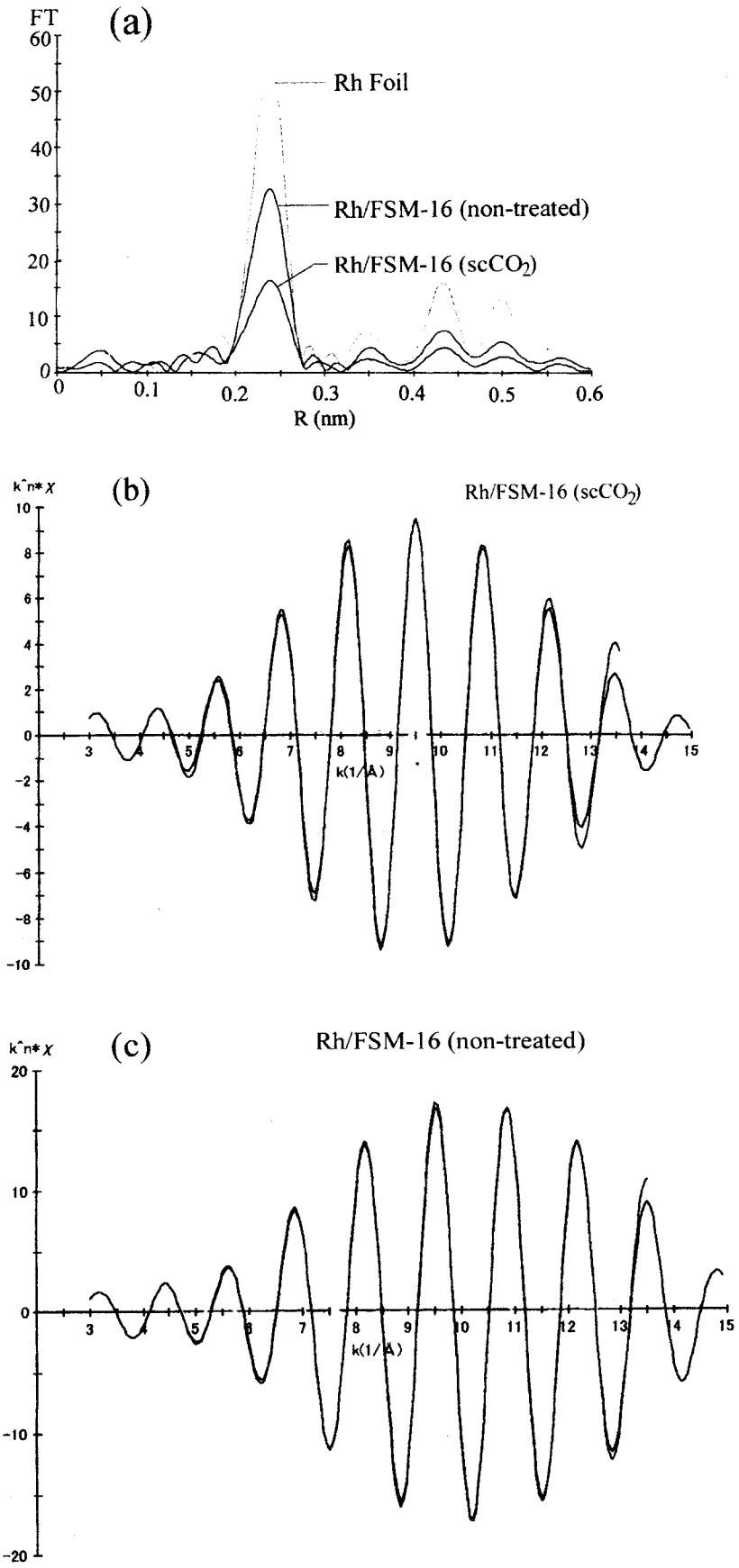

Figure 3. Results of EXAFS for Rh/FSM-16 catalysts: (a) Fourier transforms of $k^3\chi(k)$, (b) curve-fitting analysis for Rh/FSM-16 ($scCO_2$) and (c) for Rh/FSM-16 (non-treated).

Table 2
Curve-fitting analyses for the Rh–Rh first shell of Rh/FSM-16 catalysts and Rh foil

Sample	CN	R (nm)	ΔE_0 (eV)	σ (nm)	R factor (%)
Rh Foil	12.0 ± 0.3	0.269 ± 0.001	0.05	0.006	0.6
Rh/FSM-16 ($scCO_2$)	7.5 ± 0.4	0.269 ± 0.001	−0.03	0.008	0.5
Rh/FSM-16 (non-treated)	9.1 ± 0.3	0.268 ± 0.001	1.00	0.007	<0.1

suggest that the particle size of Rh is smaller for the Rh/FSM-16 ($scCO_2$) than for the Rh/FSM-16 (non-treated). After the reverse-Fourier transformation of the major peak, the curve-fitting analysis in the k space was performed (figures 3(b), (c)) and the results are summarized in table 2. The interatomic distances (R) of Rh–Rh are 0.268–0.269 nm, almost the same as that of Rh foil (0.269 nm). However, the coordination numbers (CN) are different: 7.5 for the Rh/FSM-16 ($scCO_2$) and 9.1 for the Rh/FSM-16 (non-treated). This confirms the higher dispersion and small particle formation for the Rh/FSM-16 ($scCO_2$), as expected from the CO uptake and TEM measurements. No contribution of Rh–O is observed at 0.15–0.30 nm for the catalysts.

In the IR spectroscopy of adsorbed CO (figure 4), strong peaks for linear CO frequencies were observed, while no bridging CO was observed on the two catalysts. The bands at 2092 and 2036 cm^{-1} are assignable to the symmetrical and unsymmetrical stretching mode of monovalent geminal carbonyl species $Rh(CO)_2(OSi\equiv)(HOSi\equiv)$ [21–27]. The shoulder peak observed in both catalysts at ~2108 cm^{-1} is ascribed to another $Rh(CO)_2$ species in which the fragment $(OSi\equiv)(HOSi\equiv)$ has a slightly different structure from that of the former [25–27]. The peak at

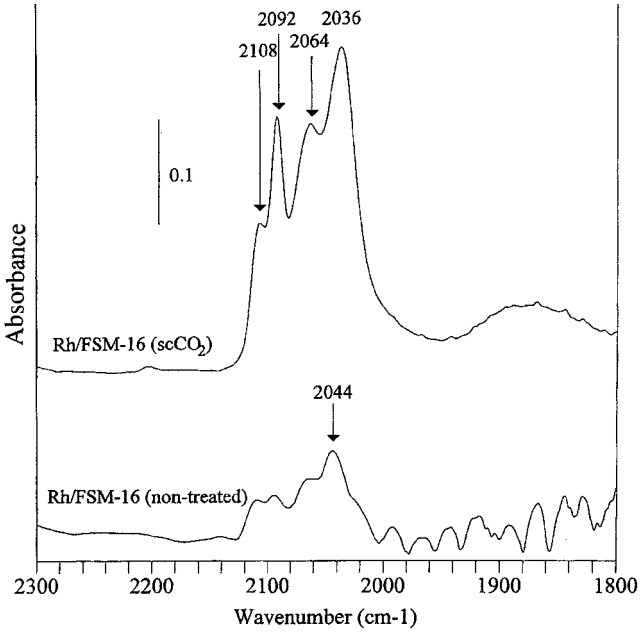

Figure 4. FTIR spectra for CO adsorption (26.6 kPa) on Rh/FSM-16 catalysts at 298 K.

2064 cm^{-1} is indicative of the linear species Rh–CO assigned to zerovalent Rh [21–24]. Yang and Garland [21] and Rice *et al.* [24] proposed that sintered Rh might give rise to linear species (Rh–CO) at 2045 cm^{-1} for low coverage of CO. We suggest that the peak at 2044 cm^{-1} for the Rh/FSM-16 (non-treated) catalyst can be attributed to this Rh–CO species. Yates *et al.* [26] reported that both linear and bridging carbonyl species are indicative of three-dimensional rhodium crystalline surfaces, while the dicarbonyl species represent atomically-dispersed Rh sites or edge sites of small two-dimensional rhodium rafts. Others [22,24] have indicated that dicarbonyl species refers to dispersed Rb atoms. This explains the difference in the IR pattern for both catalysts. As dispersion increases, Rh dicarbonyl species arise from the atomically-dispersed Rh sites or from edge sites with increase in the interaction with the support. The enhanced intensity of the 2092 cm^{-1} peak in the Rh/FSM-16 ($scCO_2$) catalyst over Rh/FSM-16 (non-treated) might indicate a greater contribution from the $Rh(CO)_2$ species in the Rh/FSM-16 ($scCO_2$) catalyst. Various authors [21,27] showed that peak intensity increases for highly dispersed rhodium. It has been reported [27,28] that highly dispersed metal particles react with CO and proton to form dicarbonyl species. The disruption of Rh–Rh bonds of small Rh crystallites is easier than on large crystallites, which gives the dicarbonyl species [27,29]. This explains the higher intensity of peaks in the Rh/FSM-16 ($scCO_2$) catalyst compared with the Rh/FSM-16 (non-treated) catalyst. It has been reported that formation of dicarbonyl species occurs on the metal centers having a slightly higher oxidation state, and hence we propose that an increase in the intensity of peaks for dicarbonyl species in the $scCO_2$-treated catalyst may come from more electron-deficient metal centers. These results lead to the conclusion that highly dispersed, slightly electron-deficient Rh particles are formed in FSM-16 after the $scCO_2$ treatment.

3.2. Hydrogenolysis of butane

Catalytic performances were probed by examining the hydrogenolysis of butane (scheme 2). In this reaction, methane, ethane and propane are produced by hydrogenolysis and isobutane is formed by isomerization.

From the catalytic results in table 3, the Rh/FSM-16 ($scCO_2$) showed higher n-butane conversions towards hydrogenolysis than the Rh/FSM-16 (non-treated) at each temperature. No isomerization of n-butane to

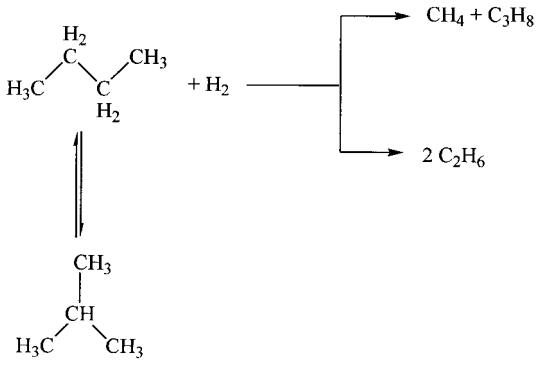

Scheme 2.

isobutane was observed on both catalysts. The carbon balance is ~100% in each catalytic run, showing no deposition of carbon on the catalyst surface. The ethane formation was enhanced in the case of Rh/FSM-16 ($scCO_2$). The difference in ethane formation is well understood by the fact that small particles exhibit higher ethane formation. Kalakkad *et al.* [19] reported this phenomenon for Rh catalysts, in which they showed the direct correlation between particle size and product distribution. It has been proposed that cleavage of the central C–C bond is favorable on small metal particles. Characterization of the catalysts throws light on understanding that small particle formation after $scCO_2$ treatment is in accord with the higher ethane formation. IR characterization shows that electron-deficient metal centers are formed on the support after $scCO_2$ treatment. It has also been proposed [19,30] that a metalacyclobutane is formed as an intermediate on Rb metal (figure 5). Increase in dispersion may increase the metal–support interaction giving rise to cationic metal centers [31]. In our case, formation of fine particles after $scCO_2$ treatment may lead to more metal–support interaction which gives rise to electron-deficient metal centers on FSM-16 support. Butane reacts with these Rh centers to form a C_2-alkene, C_2-carbene metalacyclobutane species as an intermediate on single metal atom involved in the reaction mechanism [32]. We suggest that the formation of $Rh(CH_2{=}CH_2)(=CHCH_3)$ intermediate may be more favorable than the counterpart $Rh(CH_2{=}CH{-}CH_3)(=CH_2)$ intermediate because of the electron-donation from the methyl group to the M=CH– carbene moiety, which leads to an increase in activity and C_2 formation for the Rh/FSM-16 ($scCO_2$) catalyst.

Somorjai [33] and Foger and Anderson [34] reported for Pt-catalyzed hydrogenolysis reactions that real active centers are Pt atoms of low coordination number located on apices, edges and surface defects of metal crystallites. From our XAFS results, it can be noted that the Rh/FSM-16 ($scCO_2$) catalyst has a low coordination number over the Rh/FSM-16 (non-treated) catalyst. Catalyst characterization explains the enhanced ethane formation in the Rh/FSM-16 ($scCO_2$) over Rh/FSM-16 (non-treated) catalyst. It is also discussed that small particle formation results in stronger adsorption of reaction intermediate on the metal site, which gives higher hydrogenolysis activity [32].

Table 3
Results of hydrogenolysis of butane by Rh/FSM-16 catalyst [a]

Catalyst	Temp. (K)	Conversion of n-C_4H_{10} (%)	Product distribution (%) [b]		
			CH_4	C_2H_6	C_3H_8
Rh/FSM-16 ($scCO_2$)	443	24	15	77	8
	453	45	17	74	9
	463	81	20	72	8
Rh/FSM-16 (non-treated)	443	8	23	64	13
	453	9	35	47	18
	463	22	28	57	14

[a] Rh/FSM-16: 0.15 g, 20–42 mesh, Rh 2.5 wt%; gas flow H_2 : n-C_4H_{10} = 9 : 1, total pressure 133 kPa, GHSV 3800 h^{-1}. The data were taken after 4 h of the reaction time at each reaction temperature.
[b] Product distribution is calculated as mole percentage of products. Carbon balance is ~100% in each run.

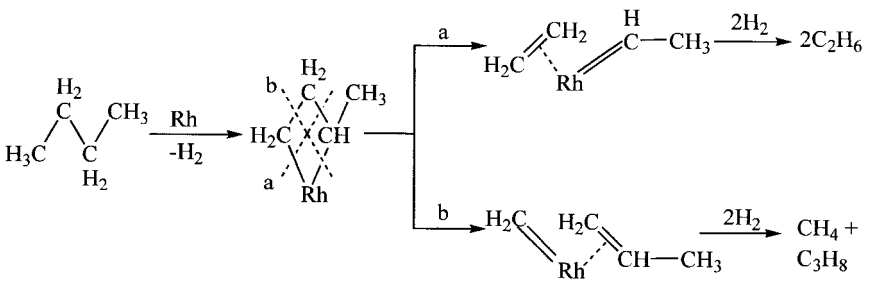

Figure 5. Reaction pathways of hydrogenolysis of butane over Rh/FSM-16 catalysts.

4. Conclusions

We have shown that the $scCO_2$ treatment is promising for preparing highly-dispersed metal particles on support. From the catalytic results on hydrogenolysis reactions, it has been pointed out that higher conversion of butane towards hydrogenolysis and high ethane formation can be achieved on the Rh/FSM-16 ($scCO_2$) catalyst. This is well correlated with the fact that, after the $scCO_2$ treatment, Rh has been homogeneously dispersed inside the mesopores of FSM-16 support, giving rise to very fine particle formation. The high diffusion property of $scCO_2$ allows metal precursors to enter the pores of FSM-16, causing the ensemble size of active Rh atoms to decrease. The CO uptake, XRD and TEM studies gave a clear idea about how the particle size and dispersion changes as we modify the way of preparation of the catalyst. The IR analysis gave information about the electron-deficient metal center, and the EXAFS characterization explains the low CN and fine particle formation after the $scCO_2$ treatment. The higher activity for the hydrogenolysis over the Rh/FSM-16 ($scCO_2$) catalyst is attributed to high dispersion, small particle size and electron-deficient metal center formation. Further applications of $scCO_2$ treatment are in progress for the preparation of supported bimetallic catalysts.

Acknowledgments

We thank Drs. H. Wakayama and Y. Fukushima, Toyota R&D Labs., for useful discussions and generous donation of FSM-16. This work was supported by a Grant-in-Aid for Scientific Research from the Ministry of Education, Science, Sports and Culture, Japan (No. 13650836).

References

[1] M. Boudart, Adv. Catal. 20 (1969) 153.
[2] B.C. Gates, *Catalytic Chemistry* (Wiley, New York, 1992) p. 387.
[3] Y. Iwasawa, *Tailored Metal Catalysts* (Reidel, Dordrecht, 1986).
[4] B.C. Gates, L. Guczi and H. Knözinger, *Metal Clusters in Catalysis* (Elsevier, Amsterdam, 1986).
[5] V. Ponec and W.M.H. Sachtler, J. Catal. 35 (1972) 250.
[6] J.R. Anderson and D.M. Mainwaring, J. Catal. 35 (1974) 162.
[7] P.G. Jessop, T. Ikariya and R. Noyori, Nature 368 (1994) 231.
[8] P.G. Jessop, T. Ikariya and R. Noyori, Chem. Rev. 99 (1999) 475.
[9] A. Baiker, Chem. Rev. 99 (1999) 453.
[10] J.A. Darr and M. Polliakoff, Chem. Rev. 99 (1999) 495.
[11] B.M. Bhanage, Y. Ikushima, M. Shirai and M. Arai, Chem. Commun. (1999) 1277.
[12] R.A. Boyse and E.I. Ko, J. Catal. 179 (1998) 100.
[13] H. Wakayama and Y. Fukushima, Chem. Commun. (1999) 391.
[14] Y. Fukushima and H. Wakayama, J. Phys. Chem. B 103 (1999) 3062.
[15] M.J. Clarke, S.M. Howdle, M. Jobling and M. Poliakoff, Inorg. Chem. 32 (1993) 5643.
[16] S. Inagaki, Y. Fukushima, K. Kuroda, J. Chem. Soc., Chem. Commun. (1993) 680.
[17] C.T. Kresge, M.E. Leonowicz, W.J. Roth, J.C. Vartuli and J.S. Beck, Nature 359 (1992) 710.
[18] S.D. Jackson, G.J. Kelly and G. Webb, Phys. Chem. Chem. Phys. 1 (1999) 2581.
[19] D. Kalakkad, S.L. Anderson, A.D. Logan, J. Pena, E.J. Braunschweig, C.H. Peden and A.K. Datye, J. Phys. Chem. 97 (1993) 1437.
[20] G. Bergeret and P. Gallezot, in: *Handbook of Heterogeneous Catalysis*, Vol. 2, eds. G. Entl, H. Knözinger and J. Weitkamp (VCH, Weinheim, 1997) p. 439.
[21] A.C. Yang and C.W. Garland, J. Phys. Chem. 61 (1957) 1504.
[22] J.T. Yates, Jr., T.M. Duncan, S.D. Warley and R.W. Vaughan, J. Chem. Phys. 70(3) (1979) 1219.
[23] M.D. Wardinsky and W.C. Hecker, J. Phys. Chem. 92 (1988) 2602.
[24] C.A. Rice, S.D. Worley, C.W. Curtis, J.A. Guin and A.R. Tarrer, J. Chem. Phys. 74 (1981) 6487.
[25] I. Burkhardt, D. Gutschick, U. Lohse and H. Miessner, J. Chem. Soc., Chem. Commun. (1987) 291.
[26] D.J.C. Yates, L.L. Murell and E.B. Prestidge, J. Catal. 57 (1979) 41.
[27] L. Schlegel, H. Miessner and D. Gutschick, Catal. Lett. 23 (1994) 215.
[28] H.F.J. Van't Blik, J.B.A.D. Van Zon, T. Huizinga, J.C. Vis, D.C. Koningsberger and R. Prins, J. Phys. Chem. 87 (1983) 2264.
[29] F. Solymosi and M. Pásztor, J. Phys. Chem. 89 (1985) 4789.
[30] E. Rodriguez, M. Leconte, J.M. Basset, K. Tanaka and K. Tanaka, J. Am. Chem. Soc. 110 (1988) 275.
[31] A.T. Bell, *Catalyst Design Progress and Perspectives* (Wiley, New York, 1987) p. 116.
[32] F. Rodríguez-Reinoso, I. Rodríguez-Ramos, C. Moreno-Castilla, A. Guerrero-Ruiz and J.D. López-González, J. Catal. 107 (1987) 1.
[33] G.A. Somorjai, *Advances in Catalysis and Related Subjects*, Vol. 26 (Academic Press, New York, 1977) p. 1.
[34] K. Foger and J.R. Anderson, J. Catal. 54 (1978) 318.